Molecular Design of Coumarin Dyes for Efficient Dye-Sensitized Solar Cells

Kohjiro Hara,[†] Tadatake Sato,[†] Ryuzi Katoh,[†] Akihiro Furube,[†] Yasuyo Ohga,[‡] Akira Shinpo,[‡] Sadaharu Suga,[‡] Kazuhiro Sayama,[†] Hideki Sugihara,[†] and Hironori Arakawa*[,†]

Photoreaction Control Research Center, National Institute of Advanced Industrial Science and Technology, 1-1-1 Higashi, Tsukuba, Ibaraki 305-8565, Japan, and Hayashibara Biochemical Laboratories, Inc., 564-176 Fujita, Okayama 701-0221, Japan

Received: September 11, 2002

We have developed novel coumarin dyes for use in dye-sensitized nanocrystalline TiO_2 solar cells (DSSCs). The absorption spectra of these novel coumarin dyes are red-shifted remarkably in the visible region relative to the spectrum of C343, a conventional coumarin dye. Introduction of a methine unit (−CH═CH−) connecting both the cyano (−CN) and carboxyl (−COOH) groups into the coumarin framework expanded the π conjugation in the dye and thus resulted in a wide absorption in the visible region. These novel dyes performed as efficient photosensitizers for DSSCs. The monochromatic incident photon-to-current conversion efficiency (IPCE) from 420 to 600 nm for a DSSC based on NKX-2311 was over 70% with the maximum of 80% at 470 nm, which is almost equal to the efficiency obtained with the N3 dye system. The IPCE performance of DSSCs based on coumarin dyes depended remarkably on the LUMO levels of the dyes, which are estimated from the oxidation potential and 0−0 energy of the dye. The slow charge recombination, on the order of micro to milliseconds, between NKX-2311 cations and injected electrons in the conduction band of TiO_2 (observed by transient absorption spectroscopy) resulted in efficient charge separation in this system. A HOMO−LUMO calculation indicated that the electron moves from the coumarin framework to the −CH═CH− unit by photoexcitation of the dye (a $\pi-\pi^*$ transition). Our results strongly suggest that molecular design of the sensitizer is essential for the construction of highly efficient DSSCs. The structure of NKX-2311, whose carboxyl group is directly connected to the −CH═CH− unit, is advantageous for effective electron injection from the dye into the conduction band of TiO_2. In addition, the cyano group, owing to its strong electron-withdrawing ability, might play an important role in electron injection in addition to a red shift in the absorption region.

Introduction

Dye-sensitized nanocrystalline TiO_2 solar cells (DSSCs) have been actively studied since Grätzel and co-workers reported high solar-cell performance with a DSSC based on a Ru-complex photosensitizer.[1,2] Several Ru complexes, e.g., *cis*-dithiocyanato bis(4,4′-dicarboxy-2,2′-bipyridine)ruthenium(II) (the N3 dye) and trithiocyanato 4,4′4"-tricarboxy-2,2′:6′,2"-terpyridine ruthenium(II) (black dye), have been used in DSSCs as efficient photosensitizers.[1−12] Ru complexes are suitable as photosensitizers for several reasons: they show a broad absorption band due to metal-to-ligand charge transfer (MLCT); the excited-states of the complexes have long lifetimes; and an oxidized Ru(III) complex has long-term chemical stability. However, the limited availability of Ru complexes will become a problem if DSSCs find wide application.

Organic dyes such as 9-phenylxanthene dyes (e.g., rose bengal, fluorescein, and rhodamine B) were also used as photosensitizers for DSSCs in early studies.[13] Recently, construction of nanocrystalline DSSCs based on organic-dye photosensitizers has been reported.[14−19] Organic dyes have several advantages as photosensitizers for DSSCs: (1) they have larger absorption coefficients (attributed to an intramolecular $\pi-\pi^*$ transition) than metal-complex photosensitizers (which are due to MLCT absorption), and these large coefficients lead to efficient light-harvesting properties; (2) the variety in their structures provides possibilities for molecular design, e.g., the introduction of substituents, and thus allows for easy control of their absorption spectra; (3) there are no concerns about resource limitations, because organic dyes do not contain noble metals such as ruthenium.

However, organic dyes have several disadvantages as photosensitizers. First, the emission lifetimes of their excited states are generally shorter than those of metal complexes (e.g., 0.4−5 ns).[20] However, if electron injection from the organic dye to the conduction band of a semiconductor occurs much faster than the dye's emission lifetime, efficient charge separation can be achieved.[21−24] A large electronic coupling between an organic dye and the conduction band of a semiconductor contributes to ultrafast electron injection.[21] Second, organic dyes have relatively sharp absorption bands in the visible region, which is disadvantage for the light harvesting of solar light. For example, DSSCs based on 9-phenylxanthene dyes such as eosin Y and mercurochrome adsorbed on TiO_2 and ZnO electrodes produced only 1.3−2.5% solar energy-to-electricity conversion efficiencies, η, under AM 1.5, whereas they showed high incident photon-to-current conversion efficiencies (IPCEs) in the range from 400 to 500 nm.[15,16] Eosin Y and mercurochrome can absorb photons and then convert them to current only at wavelengths shorter than 600 nm. Coumarin dyes, e.g., coumarin

* To whom correspondence should be addressed. Phone: +81-298-61-4410. Fax: +81-298-61-6771. E-mail: h.arakawa@aist.go.jp.
[†] National Institute of Advanced Industrial Science and Technology.
[‡] Hayashibara Biochemical Laboratories, Inc.

10.1021/jp026963x CCC: $25.00
Published on Web 12/12/2002

SCHEME 1: Molecular Structures of C343 and the Novel Coumarin Dyes, where TsO− Represents the Toluene-4-sulfonate Anion

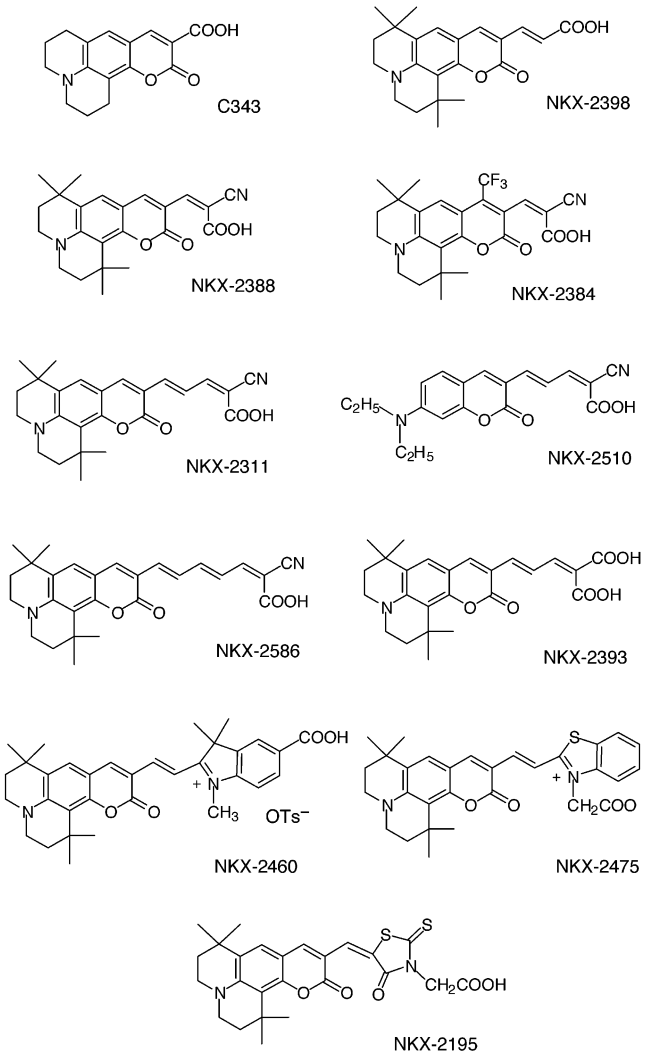

343 (C343, Scheme 1), are also good organic-dye photosensitizers for injecting electrons efficiently into the conduction band of semiconductors. Electron-transfer processes in the C343-sensitized semiconductor systems have been studied.[21−23,26−28] Ultrafast electron injection times of 20−200 fs from C343 into the conduction band of TiO_2 have been observed.[21−23] The η for nanocrystalline DSSCs based on the C343 dye, however, are lower than the efficiencies of DSSCs based on Ru-complex photosensitizers, owing to the former's lack of absorption in the visible region. Therefore, the absorption spectra of organic dyes must be broadened and red-shifted for highly efficient solar-cell performance in terms of harvesting sunlight.

Using the molecular design of organic dyes to overcome their disadvantages is essential for the construction of highly efficient DSSCs based on the dyes. Organic-dye photosensitizers used in DSSCs, must have an anchoring group (e.g., −COOH, $-SO_3H$) to be adsorbed onto the semiconductor surface with a large electronic coupling. The absorption spectra of organic dyes could be red-shifted by expansion of the π conjugation in the dyes and introduction of electron-donating and -withdrawing substituents into the dye framework; such substitutents can shift the levels of the dyes highest occupied molecular orbitals (HOMOs) and their lowest unoccupied molecular orbitals (LUMOs). Red-shifting the absorption spectrum is not the only important consideration in the design of efficient organic-dye photosensitizers; the potential levels of the HOMO and LUMO must be matched to the conduction band level of the semiconductor electrode and to the iodine redox potential. A red shift in the absorption spectrum decreases the energy gap between the HOMO and the LUMO of the dye. To accept electrons, the HOMO level must be more positive than the iodine redox potential, and to inject electrons, the LUMO level must be more negative than the conduction band level of the semiconductor. Considering these points, we have designed and synthesized novel coumarin derivatives able to absorb in the visible range from 400 to 750 nm (Scheme 1). Introduction of the methine (−CH═CH−) unit connecting the cyano (−CN) and carboxyl (−COOH) groups into the coumarin framework expanded the π conjugation in the dye and resulted in wide absorption in the visible region. We were able to construct highly efficient DSSCs based on these new coumarin photosensitizers. We reported that 5.6-6.0% η was attained under simulated AM 1.5 (100 mW cm^{-2}) with a DSSC based on 2-cyano-5-(1,1,6,6-tetramethyl-10-oxo-2,3,5,6-tetrahydro-1*H*,4*H*,10*H*-11-oxa-3a-aza-benzo[*de*]-anthracen-9-yl)-penta-2,4-dienoic acid (NKX-2311).[29,30] It has been suggested that, owing to their strong electron-withdrawing abilities, the carboxyl and cyano groups directly connected to the −CH═CH− unit play an important role in effective electron injection into the conduction band of TiO_2 in addition to red-shifting the absorption region.

In this paper, we report the details of the molecular design of these novel coumarin dyes, their photoelectrocheimical properties, and their performance in DSSCs. A detailed study of the performance of a DSSC based on NKX-2311 is also discussed. Our results strongly indicate that the molecular design of organic-dye photosensitizers for DSSCs can be successful and that the prospects for application of these photosensitizers in DSSCs are promising.

Experimental Section

1. Synthesis of Dyes. Detailed synthesis procedure of novel coumarin dyes are shown in the Supporting Information.

2. Preparation of Dye-Sensitized TiO_2 Thin Films. Detailed procedures for preparing nanocrystalline TiO_2 film electrodes have been reported elsewhere.[30] The thickness of the TiO_2 thin films, measured by an Alpha-Step 300 profiler (Tencor Instruments), was ca. 13 μm. Coumarin dyes (0.3 mM) were dissolved in a 50:50 solution of *tert*-butyl alcohol (Kanto Chemical) and acetonitrile (Kanto, dehydrated for organic synthesis). These solvents were used as obtained from the suppliers without further purification. The TiO_2 thin films were immersed into the dye solution and then kept at 25 °C for more than 12 h so that the dye could be adsorbed onto the surface of the TiO_2 electrodes: the amount of coumarin dye adsorbed on a 10-μm TiO_2 film was $1-1.2 \times 10^{-7}$ mol cm^{-2}.

3. Characterization of the Dyes. The absorption spectra of the dyes in solution and adsorbed on TiO_2 films were measured with a Shimadzu UV-3101PC. Emission spectra were measured with a Hitachi F-4500 spectrometer. FT-IR absorption spectra were measured with a Perkin-Elmer Spectrum One spectrometer in transparency mode with an ATR system equipped with a ZnSe prism. The oxidation and reduction potentials of the dyes in DMF solution were measured in a normal one-compartment cell with a glassy carbon working electrode, a Pt counter electrode, and a Ag/AgCl reference electrode in a saturated KCl solution. The measurements were performed with a Yanaco polarographic analyzer P-3000.

To measure photoluminescence lifetimes, we used a streak camera (Hamamatsu, STREAK SCOPE C4334). The excitation

TABLE 1: Absorption, Emission, and Electrochemical Properties of Coumarin Dyes

	absorption[a]		emission[b]		E_{0-0}[c]	oxidation and reduction potentials[d]	
dye	λ_{max}/nm	ϵat λ_{max}/M^{-1} cm^{-1}	λ_{max}/nm	lifetime/ns	/eV	E_{ox}/V vs NHE	E_{red}/V vs NHE
C343	442	15 100	470	4.0	2.48	1.21[22]	−1.23[22]
NKK-2398	451	45 800	505	3.5	2.25	1.20	−1.31
NKX-2388	493	44 200	540	1.7	2.18	1.35	−0.85
NKX-2384	477	22 600	600	2.3	1.98	1.46	−0.67
NKX-2510	480	49 800	535	1.4	2.05	1.42	−0.82
NKX-2311	504	51 900	560	1.9	1.97	1.28	−0.82
NKX-2393	486	42 000	520	3.0	2.07	1.16	−0.77
NKX-2586	506	59 100	610	0.9	1.85	1.15	−0.83
NKX-2195	539	52 200	580	2.5	1.85	1.22	−0.86
NKX-2460	616	103 000	490[e]	3.2	1.71	1.18	−0.35
NKX-2475	578	59 800	673	0.9	1.72	1.15	−0.57

[a] Absorption spectra were measured in methanol solution. [b] Emission spectra and lifetimes were measured in *tert*-butyl alcohol-acetonitrile (1:1) solution at 25 °C. [c] E_{0-0} values were estimated from the onset of absorption spectrum. [d] Redox potential of dyes were measured in 0.1 M tetrabutylammonium perchlorate in DMF (working electrode, glassy carbon; reference electrode, Ag/AgCl; counter electrode, Pt). [e] The emission λ_{max} at 491 nm is considered to correspond the absorption at 419 nm and no emission corresponding to the absorption λ_{max} at 616 nm was observed.

light source was the second-harmonic light (400 nm) of a femtosecond mode-locked Ti:sapphire laser (800-nm center wavelength, 50-fs pulse width, 1-Hz repetition, Spitfire, Spectra-Physics). The sample solution was placed in a quartz cell (1 cm × 1 cm), and the fluorescent light was introduced into the entrance slit of the streak camera at a 90° angle with respect to the excitation beam. The time resolution of the measurements was 30−50 ps.

Transient absorption was measured by means of the pump−probe technique. A second-harmonic pulse (532 nm, duration 8ns) from a Nd^{3+}:YAG laser (Continuum, Surelite II) was used as the pumping light. A halogen lamp (50 W) was used as a probe light source. The probe light transmitted through the sample specimen was detected with a Si photodiode (Hamamatsu, S-1722) after being dispersed with a monochromator (Acton, SpectraPro-150). We recorded the signal at a particular wavelength on a digital oscilloscope (Tektronix, TDS680C) and analyzed it by a computer to obtain the change in absorbance with time. All measurements were carried out with dye-coated TiO_2 films at room temperature without solvent.

All DFT calculations were performed with the Gaussian 98 program package. The geometries of the compounds were optimized by means of the B3LYP method in combination with the 3-21G* basis set. The nature of the stationary points was assessed by means of vibrational-frequency analysis, as were the theoretical IR absorption spectra. Vibrational frequencies predicted at the B3LYP/3-21G* level were used without scaling. All calculations were done on the IBM RS/6000-SP system at the Tsukuba Advanced Computing Center.

4. Photovoltaic Measurements of the Solar Cells. The electrochemical cell (two-electrode type) used for photovoltaic measurements consisted of a dye-sensitized semiconductor electrode, a counter electrode, a polyethylene film spacer (25 μm thick), and an organic electrolyte. The counter electrode was a Pt film sputtered on a TCO-coated glass plate by means of a sputtering system (Eiko engineering, IB-5). The apparent surface area of the TiO_2 film electrode was ca. 0.25 cm^2 (0.5 cm × 0.5 cm).

The electrolyte consisted of 0.6 M 1,2-dimethyl-3-*n*-propylimidazolium iodide (DMPImI), 0.1 M LiI, and 0.05 M I_2 in methoxyacetonitrile (MAN). Reagent-grade LiI (Wako) and I_2 (Wako) were used for the electrolyte. MAN (Aldrich and Tokyo Kasei) were distilled before use. DMPImI was synthesized from 1,2-dimethylimidazolium (Tokyo Kasei) and *n*-propyl iodide (Tokyo Kasei), as reported in a previous paper.[31]

The photovoltaic performance of the solar cells based on coumarin dyes was measured with a source meter (Advantest, R6246). We employed an AM1.5 solar simulator (Yamashita Denso Co., YSS-150A with a 1000-W Xe lamp and an AM filter) as the light source. The incident light intensity was calibrated with a standard solar cell for amorphous silicon solar cell produced by Japan Quality Assurance Organization (JQA). Action spectra of the monochromatic IPCEs for the solar cells were measured with a CEP-99W system (Bunkoh-keiki Co., Ltd.).

Results and Discussion

1. Absorption, Emission, and Electrochemical Properties of Novel Coumarin Dyes. The photoelectrochemical properties of a conventional coumarin dye, C343, and the novel coumarin dyes synthesized in this work are shown in Table 1. Figure 1a shows the absorption spectra of coumarin dyes, C343, and NKX-2388, -2311, and -2586 in ethanol. All absorption peaks for the novel coumarin dyes are shifted toward the longer-wavelength region relative to the peak for C343 (Table 1). The absorption peak for NKX-2398 (451 nm), which has a methine unit and carboxyl group on the coumarin framework, is slightly red-shifted compared to the peak for C343 (442 nm). Adding a cyano group (−C≡N) to NKX-2398, giving NKX-2388, caused a further red shift, to 493 nm. For dyes with a cyanoacetic acid unit (=C(−C≡N)−COOH) connected directly to the methine chain, the absorption spectra were considerably red-shifted by the extension of the methine chain (NKX-2388, -2311, and -2586). These results obviously indicate that connecting the cyanoacetic acid moiety to the coumarin framework via a methine chain leads to a considerable red shift in the absorption properties of the dyes, a shift that is desirable for harvesting light from the solar spectrum.

The molar absorption coefficients, ϵ, for these dyes range from 22 600 to 103 000 M^{-1} cm^{-1} (M: mol cm^{-3}) and are larger than the coefficients for C343 and Ru-complex photosensitizers.[4,6] The absorption spectrum of NKX-2311 shows a long tail spreading out to 750 nm (ϵ ca. 100), which suggests the possibility of converting 400−750-nm visible light to current using this dye. The absorption spectrum of NKX-2510, whose coumarin framework bears a diethylamino group (Scheme 1), is blue-shifted relative to the spectrum of NKX-2311, which indicates that a ring structure including an amino group in the coumarin framework (Scheme 1) is important for a red shift in the absorption spectrum of coumarin dye. Introduction of (4-oxo-2-thioxo-thiazolidin-3-yl)-acetic acid (rodanine), indolium,

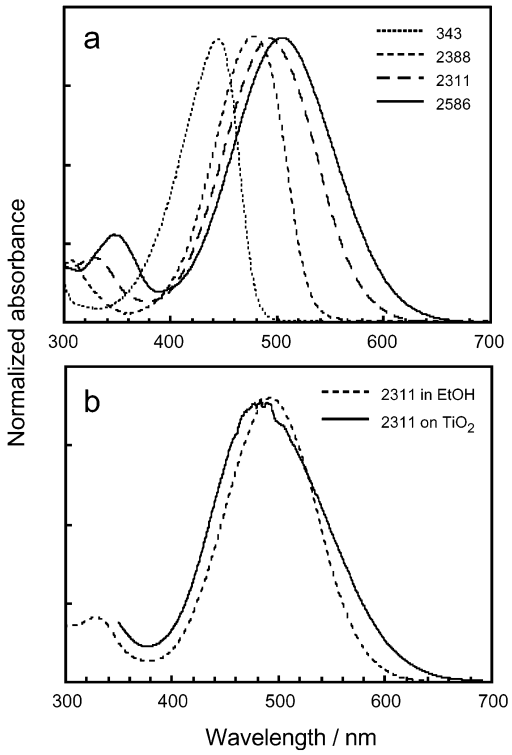

Figure 1. (a) Absorption spectra of the coumarin dyes in EtOH: (- - -) C343, (— — —) NKX-2388, (— —) NKX-2311, (—) NKX-2586. (b) (— — —) NKX-2311 in EtOH and (—) NKX-2311 adsorbed on a TiO_2 film with normalized absorbance.

and benzothiazolium moieties in π conjugation with the coumarin framework also resulted in a red shift in the absorption spectrum: λ_{max} 539 nm for NKX-2195, 616 nm for NKX-2460, and 578 nm for NKX-2475. We attribute these red shifts to the strong electron-withdrawing abilities of these three moieties, similar to the −C≡N and −COOH groups. The absorption spectrum of NKX-2311 adsorbed on a transparent TiO_2 film (4 μm thick) is broader than the spectrum in ethanol (Figure 1b). It is suggested that the broadening of the absorption spectrum is due to an interaction between the dyes and TiO_2. It has been also observed that when C343 is adsorbed onto the TiO_2 surface the absorption spectrum of the dyes becomes broad and a little red-shifted.[28]

Emission peaks and lifetimes for the coumarin dyes are shown in Table 1. The emission lifetimes of these novel coumarin dyes, ranging from 0.9 to 3.5 ns, are shorter than the lifetimes of Ru-complex photosensitizers.[4−6] As we mentioned above, if electron injection from the dye into the conduction band of TiO_2 occurs much faster than the emission lifetimes of these dyes, their shorter lifetimes will not prevent effective electron injection and consequently they act as efficient photosensitizers. Ramakrishna et al. have observed the emission with a relative longer lifetime (∼20 ns) because of the twisted intramolecular charge transfer (TICT) state of a coumarin dye, D-1421, which has a diethyl amino group.[28] No emission of the TICT state of NKX-2510, which has also a diethyl amino group, has been observed in our experiment: this might be due to the different solvent.

The oxidation and reduction potentials of the novel coumarin dyes in DMF solution are listed in Table 1. The reduction potentials for NKX-2398 and -2388, −1.31 and −0.85 V vs NHE (normal hydrogen electrode), respectively, indicate that introducing a −C≡N group shifted the reduction potential of the dye in a positive direction, because of the group's electron-withdrawing ability. This suggests that the red shift in the absorption spectrum of NKX-2388 relative to that for NKX-2398 is caused by a positive shift in the reduction potential. Introduction of an electron-withdrawing trifluoromethyl group ($-CF_3$) into the coumarin framework of NKX-2388 (producing NKX-2384) also resulted in a positive shift in the reduction potential, to −0.67 V. Lengthening the methine unit shifted the oxidation potential of the dyes negatively: 1.35 V for NKX-2388, 1.28 V for NKX-2311, and 1.15 V for NKX-2586, whereas the reduction potential remained constant (ca. −0.8 V). This result suggests that the red shift in the absorption because of the expansion of the methine unit can be attributed to negative shifts in the oxidation potentials of the dyes rather than to positive shifts in the reduction potentials. The reduction potential of NKX-2393, which has two carboxyl groups connected to the methine chain, is more positive than that for NKX-2311, which indicates the strong electron-withdrawing ability of the −COOH group. Introduction of indolium and benzothiazolium moieties in conjugation with the coumarin framework via a methine unit lead to a positive shift in the reduction potential of the resulting dyes: −0.35 V vs NHE for NKX-2460 and −0.57 V for NKX-2475 (Table 1). This shift should be caused by the strong electron-withdrawing abilities that arise from the cationic structure of these moieties.

2. Photovoltaic Performance of DSSCs Based on Coumarin Dyes. Action spectra of monochromatic IPCEs for DSSCs composed of a nanocrystalline TiO_2 electrode, novel coumarin dyes, and an iodine redox electrolyte are shown in Figure 2, parts a and b. The IPCEs are represented by the following equation:

$$\text{IPCE (\%)} = \frac{1240\ [\text{eV nm}]\ J_{ph}\ [\text{mA cm}^{-2}]}{\lambda\ [\text{nm}]\ \Phi\ [\text{mW cm}^{-2}]}\,100 \qquad (1)$$

where J_{ph} is the short-circuit photocurrent density for monochromatic irradiation and λ and Φ are the wavelength and the intensity, respectively, of the monochromatic light. As we have seen, the IPCE spectra of DSSCs based on novel coumarin dyes are remarkably red-shifted compared to the spectrum of C343. The onset of the IPCE spectrum of a DSSC based on NKX-2311 is 750 nm, and high IPCE performance (>70%) was observed in the range from 460 to 600 nm, with a maximum value of 80% at 470 nm (Figure 2a). When the reflection and absorption losses in the TCO substrate are considered, the net photon-to-current conversion efficiency in this range is higher than 90%, which is very efficient solar cell performance. In contrast, DSSCs based on NKX-2384 and -2195 showed lower IPCEs with maxima of 42% (475 nm) and 38% (540 nm), respectively (Figure 2b).

Figure 3 shows the plots of IPCEs at the λ_{max} of the novel coumarin dyes plotted as a function of the oxidation potential (E_{ox}) minus the 0−0 energy of the dyes (E_{0-0}). We consider the potential levels of $E_{ox} - E_{0-0}$ to correspond to the LUMO level of the dyes, rather than to their the reduction potential of the dyes; however, the actual LUMO levels of the dyes adsorbed on TiO_2 surface might be different from $E_{ox} - E_{0-0}$. As shown in Figure 3, DSSCs based on dyes whose $E_{ox} - E_{0-0}$ values are more negative than ca. −0.7 V vs NHE showed high IPCEs, whereas dyes whose $E_{ox} - E_{0-0}$ is more positive than −0.6 V did not exhibit high IPCEs. Electron injection from such dyes to TiO_2 would be suppressed as the energy gap between the conduction band edge level of TiO_2 and the LUMO level of the dye decreased. Consideration of the potential level of conduction band edge of TiO_2, ca. −0.5 V vs NHE,[11] suggests

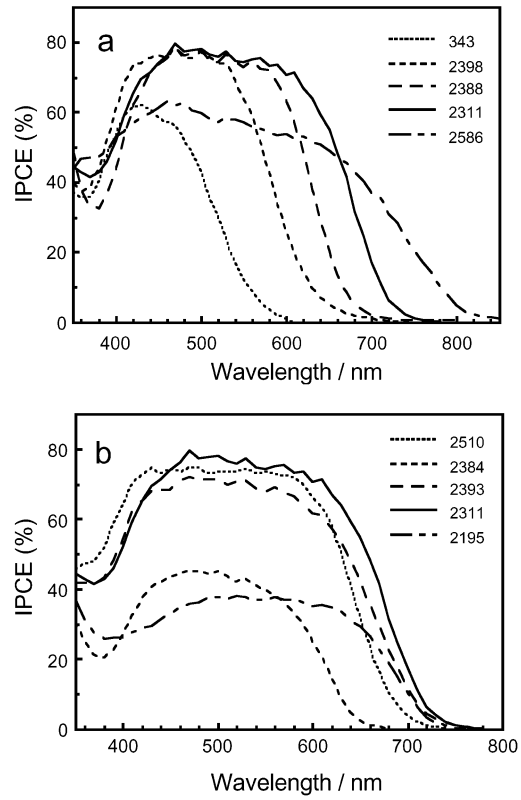

Figure 2. Spectra of monochromatic incident photon-to-current conversion efficiencies (IPCEs) for DSSCs based on coumarin-dye photosensitizers: (a) (- - -) C343, (— — —) NKX-2398, (——) NKX-2388, (—) NKX-2311, (— -) NKX-2586; (b) (- - -) NKX-2510, (— — —) NKX-2384, (— —) NKX-2393, (—) NKX-2311, (— -) NKX-2195. The electrolyte was a solution of 0.6 M DMPImI/0.1 M LiI/0.05 M I_2 in methoxyacetonitrile.

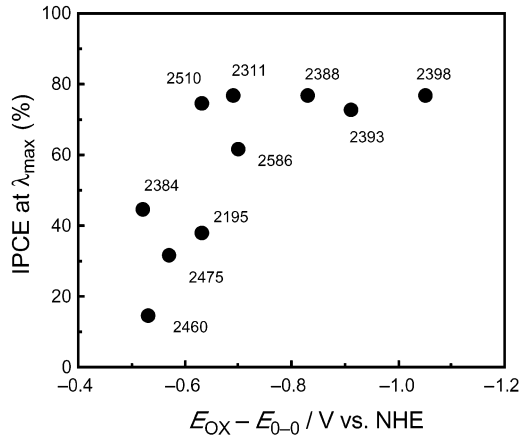

Figure 3. IPCE at λ_{max} for DSSCs based on coumarin dyes, plotted as a function of $E_{ox} - E_{0-0}$ (vs NHE) of the dyes.

that an energy gap of ca. 0.2 eV between the LUMO of the dye and the conduction band edge of TiO_2 must be a necessary driving force for effective electron injection and thus high IPCEs. Actually, in the ZnO system, transient absorption spectroscopy has revealed that electron-injection yield from NKX-2195 to ZnO is lower than that from NKX-2311.[32] The different IPCE performance for the dyes, whose values of $E_{ox} - E_{0-0}$ are almost the same (e.g., NKX-2384, -2460, -2195, and -2510), cannot be explained at the present time. In addition to the $E_{ox} - E_{0-0}$ for the dye, there seem to be several other factors that determining the IPCE performance.

We have succeeded in the most red shift in the absorption spectrum of the NKX-2311-type dyes by expansion of the methine unit of NKX-2311 (NKX-2586), as shown in Figure 2a. Therefore, it is prospective that a DSSC based on NKX-2586 shows the highest solar-cell performance in terms of light harvesting and thus the highest photocurrent. In fact, the onset of the IPCE spectrum for a DSSC based on NKX-2586 was the most red-shifted, reaching 800 nm. Its IPCE performance is, however, lower than the value for NKX-2311 (ex. the maximum is 63% at 460 nm), whereas the $E_{ox} - E_{0-0}$ of NKX-2586 differs little from that of NKX-2311 (Figure 3). It is possible that aggregates of NKX-2586 form on the TiO_2 surface and thus decrease electron-injection yield owing to intermolecular energy transfer. To suppress such dye aggregation, deoxycholic acid (DCA) derivatives have been employed as coadsorbates in DSSCs based on porphyrin,[33] phthalocyanines,[34] the black dye,[3] and a Ru phenanthroline complex,[7] and consequently, both photocurrent and photovoltage were improved. The IPCE of a DSSC based on NKX-2586 was improved when we employed DCA as a coadsorbate (data not shown), which suggests that the lower IPCE is indeed due to aggregation.

TABLE 2: Photovoltaic Performance of Coumarin Dye-sensitized Nanocrystalline TiO_2 Solar Cells

dye	J_{sc}/mA cm^{-2}	V_{oc}/V	fill factor	η/%
C343	4.1	0.41	0.56	0.9
NKX-2398	11.1	0.51	0.60	3.4
NKX-2388	12.9	0.50	0.64	4.1
NKX-2384	9.4	0.50	0.65	3.1
NKX-2510	13.2	0.53	0.67	4.7
NKX-2311	15.2	0.55	0.62	5.2
NKX-2586	15.1	0.47	0.50	3.5
NKX-2393	12.8	0.48	0.60	3.7
NKX-2195	7.5	0.49	0.70	2.6
NKX-2460	2.7	0.34	0.63	0.6
NKX-2475	4.5	0.38	0.63	1.1

[a] Conditions: irradiated light, simulated AM 1.5 (100 mW cm^{-2}); photoelectrode, TiO_2 (13 μm thickness and 0.25 cm^2); electrolyte, 0.6 M 1,2-dimethyl-3-*n*-propylimidazolium iodide/0.1 M LiI/0.05 M I_2 in methoxyacetonitrile.

Table 2 shows the photovoltaic performance of DSSCs based on coumarin dyes under AM 1.5 irradiation (100 mW cm^{-2}) using an electrolyte of 0.6 M DMPImI/0.1 M LiI/0.05 M I_2 in MAN. The solar energy-to-electricity conversion efficiency, η, under white-light irradiation (e.g., AM 1.5) can be obtained from the following equation:

$$\eta\ (\%) = \frac{J_{SC}[\text{mA cm}^{-2}]\ V_{oc}[\text{V}]\ \text{ff}}{I_0\ [\text{mW cm}^{-2}]}\ 100 \qquad (2)$$

where I_0 is the photon flux (e.g., ca. 100 mW cm^{-2} for AM 1.5), J_{sc} is the short-circuit photocurrent density under irradiation, V_{oc} is the open-circuit photovoltage, and ff represents the fill factor. As shown in Table 2, the J_{sc} values for the DSSCs depend markedly on the dyes; these values are reflected in their IPCE performance. The J_{sc} values for the DSSCs based on NKX-2311 and -2586 reached 15 mA cm^{-2}, and a 5.2% η for a DSSC based on NKX-2311 was attained (J_{sc} = 15.2 mA cm^{-2}, V_{oc} = 0.55 V, and ff = 0.62). The DSSCs based on NKX-2393 and -2586 showed relative lower V_{oc} compared to that for the DSSC based on NKX-2311, leading to lower η. At the present stage, the maximum 6.0% η was achieved by optimization under AM 1.5 with a DSSC based on NKX-2311 (J_{sc} = 14.0 mA cm^{-2}, V_{oc} = 0.60 V, and ff = 0.71).[30]

3. Mechanism of Photon-to-Current Conversion in the DSSC Based on NKX-2311. As we have seen, the DSSC based on NKX-2311 is an efficient solar cell. To better understand

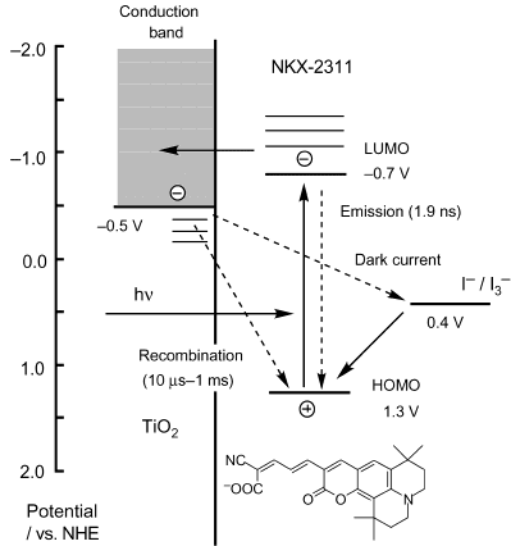

Figure 4. Schematic energy diagram for a DSSC based on NKX-2311, a nanocrystalline TiO_2 electrode, and I^-/I_3^- redox electrolyte. The oxidation potential (E_{ox}) and $E_{ox} - E_{0-0}$ for NKX-2311 are used as energy levels for the HOMO and LUMO, respectively.

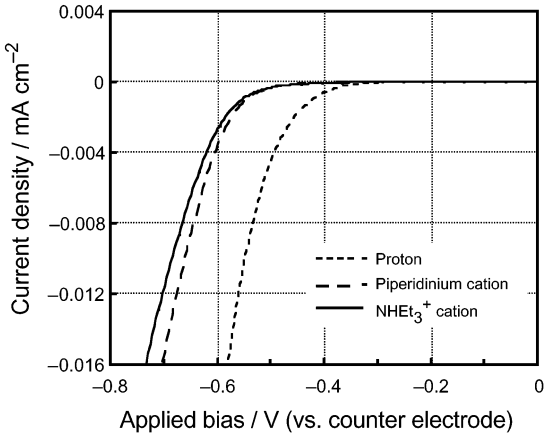

Figure 5. Current−potential curves obtained for NKX-2311-sensitized TiO_2 solar cells in the dark in an electrolyte of 0.6 M DMPImI/0.1 M LiI/0.05 M I_2 in methoxyacetonitrile: (− − −) proton, (− −) piperidinium cation, (—) triethylhydroammonium ($NHEt_3^+$) cation. The applied bias vs the Pt counter electrode is plotted on the *x* axis.

the photon-to-current conversion mechanism for this DSSC and to improve the solar-cell performance, we investigated this system in detail. We studied the system's charge recombination kinetics, the structure of NKX-2311 adsorbed on TiO_2, and the improvement of photovoltage due to ammonium countercations.

Figure 4 shows a typical energy diagram for a DSSC based on a nanocrystalline TiO_2 electrode, NKX-2311 as photosensitizer, and the I^-/I_3^- redox electrolyte. The HOMO and LUMO levels of the dye correspond to the oxidation potentials of the dye and its $E_{ox} - E_{0-0}$ level, respectively. As mentioned above, the energy levels of the free dye might differ from the levels for the dye adsorbed on the TiO_2 surface. The following primary steps are involved in the conversion of photons to current. NKX-2311 adsorbed on the TiO_2 surface absorbs the incident photon flux and is then excited from the ground state to the excited-state owing to the intramolecular $\pi-\pi^*$ transition. The electron of the excited state is immediately injected into the conduction band of the TiO_2 electrode before it is deactivated by emission (1.9 ns lifetime) and subsequent formation of the oxidized dye (i.e., the dye cation). Injected electrons in the conduction band of TiO_2 are transported toward the back contact (TCO). The oxidized dyes accept electrons from the I^- redox mediator, regenerating the ground state of the dye, and I^- is oxidized to I_3^-. There are two main loss processes that determine the performance of a DSSC: recombination (i.e., reduction of the oxidized dye by the injected electrons on TiO_2) and dark current, which corresponds to reduction of I_3^- by the injected electrons (Figure 4). Therefore, the injected electrons must be transported to the backcontact before these processes can occur.

It has been reported that charge recombination between injected electrons on TiO_2 and the oxidized N3 dye occurs on the order of microseconds to milliseconds[35] and that electron injection from the N3 dye into TiO_2 occurs on the order of femtoseconds to picoseconds.[35−39] For effective charge separation, the charge recombination process must be much slower than electron transfer from I^- to the oxidized dyes (i.e., rereduction of the dye cations, Figure 4). It has been reported that charge recombination between injected electrons on TiO_2 and the oxidized N3 dye is much slower than rereduction of the dye cations with I^- (100 ns),[40] whereas the recombination rate increases under applied negative bias at which the solar cell is performed under irradiation.[40]

As we mentioned, the solar cell based on NKX-2311 and TiO_2 performs efficiently, which suggests that effective charge separation occurs in this system. We have investigated the decay profile of transient absorption of bleach of absorption due to production of NKX-2311 cations on a TiO_2 film monitored at 600 nm: an excitation at 532 nm with an intensity of 0.1 mJ cm^{-2}. The bleaching of the ground-state absorption of NKX-2311 recovered over a time range from 10 μs to 1 ms, which indicates that charge recombination between the NKX-2311 cations and the injected electrons on TiO_2 is a slow process, as it is in the N3 dye system: the recombination rate depends on the TiO_2 films used in the experiment. The rereduction of the N3 dye cations by I^- occurs within 100 ns.[40] Although no experimental data are available for NKX-2311, rereduction of NKX-2311 cations by I^- should occur much faster than the recombination process, just as in the N3 dye system. A slow recombination process would contribute to efficient charge separation and thus result in high solar-cell performance for DSSCs based on the coumarin dyes. Details of the charge recombination kinetics in this system (e.g., effect of applied negative bias) are now under investigation and the results will be reported.

4. Improvement of Photovoltage with Ammonium Countercations. Replacement of two of the four carboxyl groups of the N3 dye by tetrabutylammonium (TBA) cations affords the so-called N719 dye, which has been also used as a photosensitizer.[4] In light of these results, we investigated the effect of the countercation of the carboxyl group in the coumarin dye system on the photovoltaic performance of the solar cell. The dyes used were NKX-2311 with a proton (H^+), a piperidinium ion, or a triethylhydroammonium ion ($NHEt_3^+$) as the countercation for the carboxyl group. Dark current properties for DSSCs based on these three types of dyes are shown in Figure 5. The onset of dark current for DSSCs based on dyes with piperidinium and $NHEt_3^+$ cations are shifted negatively compared to the onset for a DSSC based on a proton-type dye, which indicates that dark current is suppressed in DSSCs based on dyes with piperidinium and $NHEt_3^+$ cations. Consequently the V_{oc} values under AM 1.5 for these solar cells were increased relative to the value for a DSSC based on a proton-type dye. We suggest that the ammonium cations exist around the TiO_2 surface after dye adsorption and that the resulting suppression

of dark current, owing to a blocking effect, leads to an improved V_{oc}. In a previous report, we discussed our investigation of the effect of TBA cations on the photovoltaic performance for solar cells based on Ru−phenanthroline complex photosensitizers.[7,42] The absorbed photon-to-current conversion efficiency (APCE) for a DSSC based on the Ru−phenanthroline complex, in which two protons of the carboxyl groups are replaced by two TBA cations, was higher than that for a four-proton-type complex, whereas the electron-injection yields from two-proton- and four-proton-type dyes into TiO_2 were almost the same.[42] This result supports the conclusion that the TBA cation suppresses dark current around the TiO_2 surface, rather than improving the electron-injection yield from the dye. Using FT-IR absorption spectroscopy, Nazeeruddin et al. concluded that some TBA cations that were dissociated from the Ru complex are adsorbed on the TiO_2 surface.[43]

Although the V_{oc} was improved when ammonium cations were employed, the J_{sc} values for DSSCs based on dyes with piperidinium and $NHEt_3^+$ cations were lower than the value for a DSSC based on a proton-type dye. We consider that protons dissociated from the carboxyl group of a proton-type-dye shifted the conduction band of TiO_2 positively, and thus lower V_{oc}. Therefore, a positive shift of the conduction band of TiO_2 does not occur in the ammonium-cation-type dyes; the lack of a positive shift leads to a smaller driving force for electron injection from the dye and consequently decreased J_{sc} value relative to that for a proton-type-dye. This interpretation is consistent with a report that the IPCE value (i.e., photocurrent) of the DSSC based on the N3 dye decreased as the number of TBA cations on the carboxyl groups of the N3 dye increased.[4]

5. FT-IR Measurements and Calculation Analysis of Dye Structure. The structure of a dye on the TiO_2 surface has a significant effect on solar-cell performance. It is suggested that NKX-2311 is adsorbed on the TiO_2 surface with a large electronic coupling, which results in a high electron-injection yield. To understand the structure of the adsorbed dye on the TiO_2 surface, we performed FT-IR absorption measurements and a calculation analysis on NKX-2311.

To model the electronic state of NKX-2311 adsorbed on the TiO_2 surface, we employed the dye's potassium salt because the dye must be bonded to the TiO_2 surface in its carboxylate form (the structural change induced by adsorption will be discussed in detail later). FT-IR absorption spectroscopy and calculation analyses have supported the notion that organic and inorganic compounds having one or more carboxyl groups are adsorbed onto the metal and metal-oxide surfaces with bidentate carboxylate coordination.[44] We optimized the geometry of NKX-2311 using the B3LYP method with the 3-21G* basis set. Figure 6 shows the calculated molecular structure of NKX-2311 and the electron distribution of its HOMO and LUMO. A series of calculations designed to find the most stable conformation showed that steric repulsion between the oxygen atom of the C═O group in the coumarin framework and the nitrogen atom of the −C≡N group makes the structure in which the −C≡N group is farthest from the carbonyl group in the coumarin framework (Figure 6) the most stable. Comparison of the electron distribution in the frontier MOs reveals that HOMO−LUMO excitation moved the electron distribution from the coumarin framework to the methine moiety. Consequently, electrons are injected into TiO_2 via the carboxyl group directly connected to the methine moiety. Therefore, this carboxyl group is important for effective electron transfer in this system. The change in electron distribution induced by photoexcitation is considered to be one of the factors determining efficient charge separation in this system.

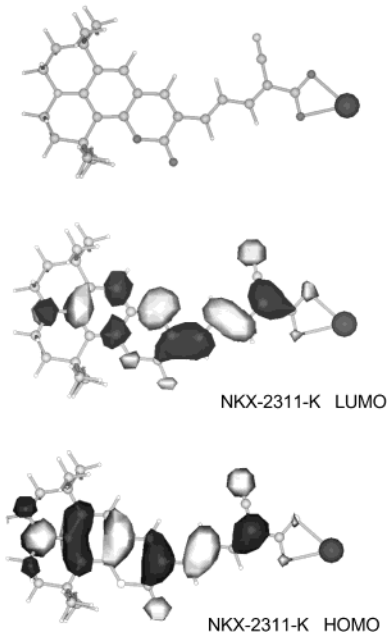

Figure 6. Structure and HOMO and LUMO of the potassium salt of NKX-2311 optimized at the B3LYP/3-21G* level.

The FT-IR absorption spectra of NKX-2311 are shown in Figure 7. In the spectrum of the neat NKX-2311-COOH (Figure 7a), the absorption peak at 2217 cm^{-1} is ascribed to the C≡N stretching band. Absorption peaks at 1710 and 1675 cm^{-1} are assigned to the C═O stretching bands of the coumarin-framework carbonyl group and the carboxyl group, respectively. In the spectrum of NKX-2311-$COONHEt_3$ (Figure 7b), the absorption assigned to the C═O stretching band (1675 cm^{-1}) has disappeared, and a new absorption band is observed at 1580 cm^{-1}, which is assigned to O−C−O asymmetric stretching in the carboxylate (−COO−). The IR absorption spectrum of NKX-2311 adsorbed on a TiO_2 film (Figure 7c) shows one C═O stretching band at 1720 cm^{-1} and an absorption at 1580 cm^{-1}, which suggests that the NKX-2311 is adsorbed onto the TiO_2 surface in its carboxylate form. In addition, we observed differences in the FT-IR-ATR spectra of the COOH- and $COONHEt_3$-types of NKX-2311 in the range from 1200 to 1600 cm^{-1} (Figure 7, parts a and b), differences that reflect the structural fluctuation in the mainframework of the NKX-2311 induced by the change from −COOH to −COO− (i.e., by deprotonation). In this wavenumber region, the spectrum of NKX-2311 on the TiO_2 surface is also more similar to the spectrum of the $NHEt_3$ salt of NKX-2311 (Figure 7b) than to the spectrum of the COOH type (Figure 7a). This result strongly suggests that NKX-2311 is adsorbed on the TiO_2 surface with a carboxylate coordination after deprotonation rather than with esterlike bonding. It has been reported that organic-dye and inorganic-dye photosensitizers are adsorbed onto TiO_2 and ZnO surfaces with carboxylate coordination[7,17,43,45−47] or esterlike bonding or both.[43,45,46] The absorption of the C≡N (2220 cm^{-1}) and C═O (1720 cm^{-1}) stretching bands changed to broad peaks owing to adsorption on the TiO_2 surface, which indicates an interaction between the dye and TiO_2 (Figure 7c).

The theoretical IR absorption spectra of NKX-2311-COOH and -COOK (i.e., the carboxylate) obtained by vibrational-frequency analysis (Figure 8, parts a and b) are in good agreement with those of NKX-2311-COOH and -$COONHEt_3$ types, respectively. Moreover, the latter corresponds well to that

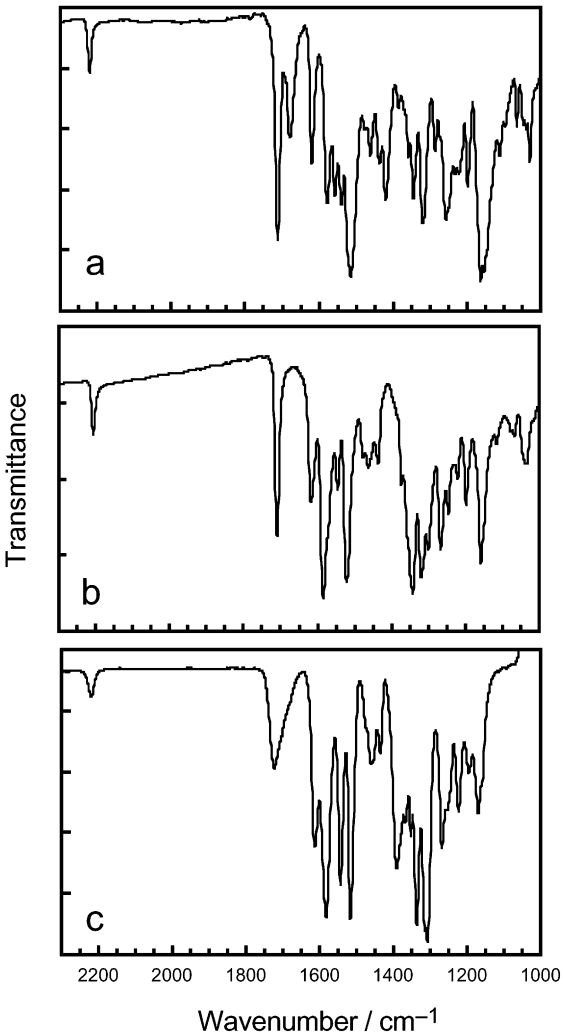

Figure 7. FT-IR absorption spectra of NKX-2311 measured by ATR equipment with a ZnSe prism: (a) neat neutral NKX-2311 (carboxylic acid type), (b) neat NKX-2311 $NHEt_3^+$ salt, and (c) NKX-2311 adsorbed on a TiO_2 film.

of NKX-2311 adsorbed on TiO_2. Therefore, the obtained geometries of NKX-2311-COOH and -$COONHEt_3$ should be good models for the molecular structures of the neutral NKX-2311 and the adsorbed NKX-2311, respectively. Figure 9 shows geometries of NKX-2311 optimized at the B3LYP/3-21G* level. The carbon−carbon bond length in NKX-2311 changed slightly when the carboxyl group (−COOH) was replaced by the carboxylate form (−COOK). A similar change would be also induced by adsorption of the dye onto the TiO_2 surface. From the experimental and theoretical IR-absorption data and the calculated molecular structure, we conclude that NKX-2311 is adsorbed on the TiO_2 surface in its carboxylate form and that its structure is slightly changed by deprotonation.

6. Perspectives. At the present stage, the maximum 6.0% η was achieved by optimization under AM 1.5 with a DSSC based on NKX-2311 (J_{sc} = 14.0 mA cm^{-2}, V_{oc} = 0.60 V, and ff = 0.71).[30] This result indicates that the prospects for using organic-dye photosensitizers in DSSCs are promising. This solar cell has the potential to produce 8−9% efficiencies because its spectral response is almost equal to that for a DSSC based on the N3 dye (or the N719 dye). To attain 8−9% efficiencies, however, we must overcome several problems. For example, a lower V_{oc} prevents the achievement of efficiencies higher than 6%. One of the reasons for this is that additives, such as *tert*-butylpyridine (TBP), that improve V_{oc} cannot be employed,

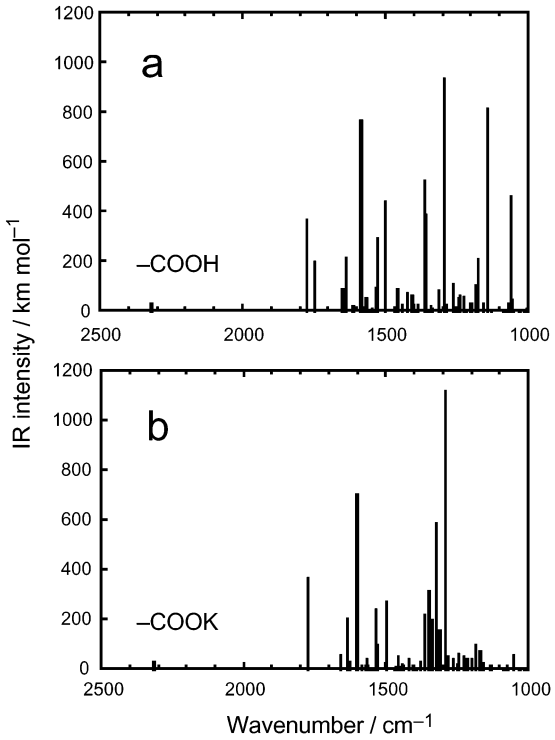

Figure 8. Theoretical IR absorption spectra of NKX-2311 obtained by vibrational-frequency analysis at the B3LYP/3-21G* level: (a) −COOH type and (b) −COOK type. Vibrational frequencies predicted at the level were used without scaling.

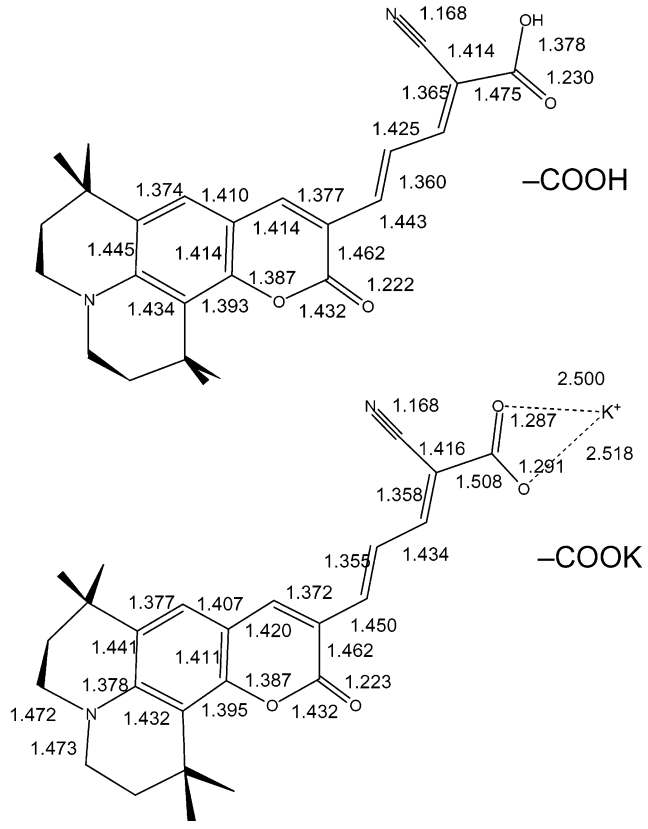

Figure 9. Geometries of NKX-2311 optimized at the B3LYP/3-21G* level: (a) −COOH type and (b) −COOK type. Bond lengths are in angstroms.

because they drastically decreases the J_{sc} value in this system, which results in the lower total efficiencies.[30] We believe that TBP negatively shifts the conduction band level of the TiO_2

electrode and consequently decreases J_{sc}. To improve V_{oc} by addition of TBP, we must design new dyes whose LUMO levels are more negative than the LUMO level of NKX-2311. Because a negative shift in the LUMO level, which leads to a blue shift in the absorption spectrum of NKX-2311, is not desirable for light harvesting of the solar spectrum, both the HOMO and LUMO levels must be shifted negatively.

Moreover, there is a problem with dark current in DSSCs based on organic-dye photosensitizers. Dark current seems to occur more readily in DSSCs based on organic-dye photosensitizers than in DSSCs based on Ru-complex photosensitizers, although the detailed mechanism is unclear at the present time. For example, the improvement in V_{oc} caused by the addition of TBP to the electrolyte in the DSSC based on NKX-2311 is smaller than that in DSSCs with Ru-complex photosensitizers (data not shown). It is possible that dark current depends strongly on the molecular structure of the photosensitizers and that organic dye adsorbed on the TiO_2 surface promotes dark current. Organic-dye photosensitizers that are designed to prevent dark current will be important for the achievement of solar-cell performance higher than 6%. We are currently designing and synthesizing new organic-dye photosensitizers to improve solar-cell performance.

Conclusions

Introduction of the −CH═CH− unit connecting both the cyano (−C≡N) and carboxyl (−COOH) groups into the coumarin framework expanded the π conjugation in the dye and resulted in wide absorption in the visible region (NKX-2388, -2311, and -2586). These dyes performed as efficient photosensitizers for DSSCs. In contrast, DSSCs based on NKX-2384, -2195, -2460, and -2475 showed low solar-cell performance owing to relative positive LUMO levels of the dyes. The onset of the IPCE spectrum for a DSSC based on NKX-2311 was 750 nm, and IPCEs higher than 70% were observed in the range from 460 to 600 nm. An IPCE spectrum for a DSSC based on NKX-2586 was expanded to 850 nm, but the maximum IPCE was low (63% at 460 nm) compared to the maxima for other DSSCs. A slow charge recombination, on the order of micro- to milliseconds, between the NKX-2311 cations and the injected electrons on TiO_2 was observed by transient absorption spectroscopy. The ammonium countercations on the carboxyl group of the dye improved the photovoltage of the DSSC based on NKX-2311. Both FT-IR absorption spectroscopy and a calculation analysis indicated that NKX-2311 is adsorbed on the TiO_2 surface with bidentate carboxylate coordination rather than with an esterlike bonding form. A HOMO−LUMO calculation indicated that an electron moves from the coumarin framework to the −CH═CH− unit, owing to photoexcitation of the dye (a $\pi-\pi^*$ transition). Our results strongly support the prospects for successful application of DSSCs based on organic-dye photosensitizers and indicate the importance of molecular structure design for tuning photosensitizers to produce highly efficient DSSCs.

Acknowledgment. This work was supported by Japan's Ministry of Education, Culture, Sports, Science and Technology, Center of Excellence Development (COE) Project, and the New Energy and Industrial Technology Development Organization (NEDO) under Ministry of Economy Trade and Industry.

Supporting Information Available: Detailed synthesis procedure of novel coumarin dyes. This material is available free of charge via the Internet at http://pubs.acs.org.

References and Notes

(1) O'Regan, B.; Grätzel, M. *Nature* **1991**, *353*, 737−740.

(2) Nazeeruddin, M. K.; Kay, A.; Rodicio, I.; Humphry-Baker, R.; Muller, E.; Liska, P.; Vlachopoulos, N.; Grätzel, M. *J. Am. Chem. Soc.* **1993**, *115*, 6382−6390.

(3) (a) Nazeeruddin, Md. K.; Péchy, P.; Grätzel, M. *Chem. Commun*. **1997**, 1705−1706. (b) Nazeeruddin, M. K.; Péchy, P.; Renouard, T.; Zakeeruddin, S. M.; Humphry-Baker, R.; Comte, P.; Liska, P.; Cevey, L.; Costa, E.; Shklover, V.; Spiccia, L.; Deacon, G. B.; Bignozzi, C. A.; Grätzel, M. *J. Am. Chem. Soc*. **2001**, *123*, 1613−1624.

(4) Nazeeruddin, Md. K.; Zakeeruddin, S. M.; Humphry-Baker, R.; Jirousek, M.; Liska, P.; Vlachopoulos, N.; Shklover, V.; Fischer, C.-H.; Grätzel, M. *Inorg. Chem*. **1999**, *38*, 6298−6305.

(5) Argazzi, R.; Bignozzi, C. A.; Heimer, T. A.; Castellano, F. N.; Meyer, G. J. *Inorg. Chem*. **1994**, *33*, 5741−5749.

(6) (a) Sugihara, H.; Singh, L. P.; Sayama, K.; Arakawa, H.; Nazeeruddin, Md. K.; Grätzel, M. *Chem. Lett*. **1998**, 1005−1006. (b) Yanagida, M.; Singh, L. P.; Sayama, K.; Hara, K.; Katoh, R.; Islam, A.; Sugihara, H.; Arakawa, H.; Nazeeruddin, Md. K.; Grätzel, M. *J. Chem. Soc., Dalton Trans*. **2000**, 2817−2822.

(7) Hara, K.; Sugihara, H.; Tachibana, Y.; Islam, A.; Yanagida, M.; Sayama, K.; Arakawa, H.; Fujihashi, G.; Horiguchi, T.; Kinoshita, T. *Langmuir* **2001**, *17*, 5992−5999.

(8) Smestad, G.; Bignozzi, C.; Argazzi, R. *Sol. Energy Mater. Sol. Cells* **1994**, *32*, 259−272.

(9) Hagfeldt, A.; Grätzel, M. *Chem. Rev*. **1995**, *95*, 49−68.

(10) Huang, S. Y.; Schlichthörl, G.; Nozik, A. J.; Grätzel, M.; Frank, A. J. *J. Phys. Chem*. **1997**, *101*, 2576−2582.

(11) Kalyanasundaram, K.; Grätzel, M. *Coord. Chem. Rev*. **1998**, *77*, 347−414.

(12) Hagfeldt, A.; Grätzel, M. *Acc. Chem. Res*. **2000**, *33*, 269−277.

(13) For example: (a) Gerischer, H.; Michel-Beyerle, M. E.; Rebentrost, F.; Tributsch, H. *Electrochim. Acta* **1968**, *13*, 1509−1515. (b) Gerischer, H.; Tributsch, H. *Ber. Bunsen-Ges. Phys. Chem*. **1968**, *72*, 437−445. (c) Watanabe, T.; Fujishima, A.; Tatsuoki, O.; Honda, K. *Bull. Chem. Soc. Jpn*. **1976**, *49*, 8−11. (d) Tsubomura, H.; Matsumura, M.; Nomura, Y.; Amamiya, T. *Nature* **1976**, *261*, 402−403.

(14) Ferrere, S.; Zaban, A.; Gregg, B. A. *J. Phys. Chem*. **1997**, *101*, 4490−4493.

(15) Sayama, K.; Sugino, M.; Sugihara, H.; Abe, Y.; Arakawa, H. *Chem. Lett*. **1998**, 753−754.

(16) (a) Hara, K.; Horiguchi, T.; Kinoshita, T.; Sayama, K.; Sugihara, H.; Arakawa, H. *Chem. Lett*. **2000**, 316−317. (b) Hara, K.; Horiguchi, T.; Kinoshita, T.; Sayama, K.; Sugihara, H.; Arakawa, H. *Sol. Energy Mater. Sol. Cells* **2000**, *64*, 115−134.

(17) (a) Sayama, K.; Hara, K.; Mori, N.; Satsuki, M.; Suga, S.; Tsukagoshi, S.; Abe, Y.; Sugihara, H.; Arakawa, H. *Chem. Commun*. **2000**, 1173−1174. (b) Sayama, K.; Tsukagoshi, S.; Hara, K.; Ohga, Y.; Shinpou, A.; Abe, Y.; Suga, S.; Arakawa, H. *J. Phys. Chem. B* **2002**, *106*, 1363−1371.

(18) (a) Wang, Z.-S.; Li, F.-Y.; Huang, C.-H. *Chem. Commun*. **2000**, 2063−2064. (b) Wang, Z.-S.; Li, F.-Y.; Huang, C.-H.; Wang, L.; Wei, M.; Jin, L.-P.; Li, N.-Q. *J. Phys. Chem. B* **2000**, *104*, 9676−9682.

(19) Sayama, K.; Hara, K.; Tsukagoshi, S.; Abe, Y.; Ohga, Y.; Shinpo, A.; Suga, S.; Arakawa, H. *New J. Chem.* **2001**, *25*, 200−202.

(20) (a) Moser, J.; Grätzel, M. *J. Am. Chem. Soc.* **1984**, *106*, 6557−6564. (b) Nasr, C.; Liu, D.; Hotchandani, S.; Kamat, P. V. *J. Phys. Chem*. **1996**, *100*, 11054−11061. (c) Khazraji, A. C.; Hotchandani, S.; Das, S.; Kamat, P. V. *J. Phys. Chem. B* **1999**, *103*, 4693−4700.

(21) Rehm, J. M.; McLendon, G. L.; Nagasawa, Y.; Yoshihara, K.; Moser, J.; Grätzel, M. *J. Phys. Chem*. **1996**, *100*, 9577−9578.

(22) Murakoshi, K.; Yanagida, S.; Capel, M.; Castner, E. W. Jr. *Interfacial Electron Transfer Dynamics of Photosensitized Zinc Oxide Nanoclusters*; Moskovits, M., Ed.; ACS: Washington, DC, 1997; pp 221−238.

(23) Ghosh, H. N.; Asbury, J. B.; Lian, T. *J. Phys. Chem. B* **1998**, *102*, 6482−6486.

(24) Hilgendorff, M.; Sundström, V. *Chem. Phys. Lett*. **1998**, *287*, 709−713.

(25) Benkö, G.; Hilgendorff, M.; Yartsev, A. P.; Sundström, V. *J. Phys. Chem. B* **2001**, *105*, 967−974.

(26) Moser, J. E.; Grätzel, M. *Chem. Phys*. **1993**, *176*, 493−500.

(27) Ghosh, H. N. *J. Phys. Chem. B* **1999**, *103*, 10382−10387.

(28) Ramakrishna, G.; Ghosh, H. N. *J. Phys. Chem. A* **2002**, *106*, 2545−2553.

(29) Hara, K.; Sayama, K.; Ohga, Y.; Shinpo, A.; Suga, S.; Arakawa, H. *Chem. Commun*. **2001**, 569−570.

(30) Hara, K.; Tachibana, Y.; Ohga, Y.; Shinpo, A.; Suga, S.; Sayama, K.; Sugihara, H.; Arakawa, H. *Sol. Energy Mater. Sol. Cells*, in press.

(31) Bonhôte, P.; Dias, A. P.; Papageorgiou, N.; Kalyanasundram, K.; Grätzel, M. *Inorg. Chem*. **1996**, *35*, 1168−1178.

(32) Katoh, R.; Furube, A.; Hara, K.; Murata, S.; Tachiya, M.; Arakawa, H. *J. Phys. Chem. B*, in press.

(33) Kay, A.; Grätzel, M. *J. Phys. Chem*. **1993**, *97*, 6272−6277.

(34) (a) Nazeeruddin, Md. K.; Humphry-Baker, R.; Grätzel, M.; Murrer, B. A. *Chem. Commun*. **1998**, 719−720. (b) He, J.; Benkö, G.; Korodi, F.; Polívka, T.; Lomoth, R.; Åkermark, B.; Sun, L.; Hagfeldt, A.; Sundström, V. *J. Am. Chem. Soc*. **2002**, *124*, 4922−4932.

(35) Tachibana, Y.; Moser, J. E.; Grätzel, M.; Klug, D. R.; Durrant, J. R. *J. Phys. Chem*. **1996**, *100*, 20056−20062.

(36) Hannappel, T,; Burfeindt, B.; Storck, W.; Willig, F. *J. Phys. Chem. B* **1997**, *101*, 6799−6802.

(37) Ellingson, R. J.; Asbury, J. B.; Ferrere, S.; Ghosh, H. N.; Sprague, J. R.; Lian, T.; Nozik, A. J. *J. Phys. Chem. B* **1998**, *102*, 6455−6458.

(38) Asbury, J. B.; Hao, E.; Wang, Y.; Ghosh, H. N.; Lian, T. *J. Phys. Chem. B* **2001**, *105*, 4545−4557.

(39) Benkö, G.; Kallioinen, J.; Korppi-Tommola, J. E. I.; Yartsev, A. P.; Sundström, V. *J. Am. Chem. Soc*. **2002**, *124*, 489−493.

(40) Haque, S. A.; Tachibana, Y.; Klug, D. R.; Durrant, J. R. *J. Phys. Chem. B* **1998**, *102*, 1745−1749.

(41) Haque, S. A.; Tachibana, Y.; Willis, R. L.; Moser, J. E.; Grätzel, M.; Klug, D. R.; Durrant, J. R. *J. Phys. Chem. B* **2000**, *104*, 538−547.

(42) Hara, K.; Horiuchi, H.; Katoh, R.; Singh, L. P.; Sugihara, H.; Sayama, K.; Murata, S.; Tachiya, M.; Arakawa, H. *J. Phys. Chem. B* **2002**, *106*, 374−379.

(43) Nazeeruddin, Md. K.; Amirnasr, M.; Comte, P.; Machay, J. R.; McQuillan, A. J.; Houriet, R.; Grätzel, M. *Langmuir* **2000**, *16*, 8525−8528.

(44) For example: (a) Szymanski, M. A.; Gillan, M. J. *Surf. Sci*. **1996**, *367*, 135−148. (b) Shklover, V.; Ovchinnikov, Y. E.; Braginsky, L. S.; Zakeeruddin, S. M.; Grätzel, M. *Chem. Mater*. **1998**, *10*, 2533−2541. (c) Patthey, L.; Rensmo, H.; Persson, P.; Westermark, K.; Vayssieres, L.; Stashans, A.; Petersson, Å.; Brühwiler, P. A.; Siegbahn, H.; Lunell, S.; Marternsson, N. *J. Chem. Phys*. **1999**, *110*, 5913−5918. (d) Han, S. W.; Joo, S. W.; Ha, T. H.; Kim, Y.; Kim, K. *J. Phys. Chem. B* **2000**, *104*, 11987−11995.

(45) Murakoshi, K.; Kano, G.; Wada, Y.; Yanagida, S.; Miyazaki, H.; Matsumoto, M.; Murasawa, S. *J. Electroanal. Chem*. **1995**, *396*, 27−34.

(46) Finnie, K. S.; Bartlett, J. R.; Woolfrey, J. L. *Langmuir* **1998**, *14*, 2744−2749.

(47) Keis, K.; Lindgren, J.; Lindquist, S.-E.; Hagfeldt, A. *Langmuir* **2000**, *16*, 4688−4694.